Atmos. Chem. Phys. Discuss., 11, 19639–19682, 2011
www.atmos-chem-phys-discuss.net/11/19639/2011/
doi:10.5194/acpd-11-19639-2011

Atmospheric Chemistry and Physics Discussions

Sources and atmospheric processing of organic aerosol in the Mediterranean: insights from aerosol mass spectrometer factor analysis

L. Hildebrandt[1], **E. Kostenidou**[2], **V. A. Lanz**[3], **A. S. H. Prevot**[3], **U. Baltensperger**[3], **N. Mihalopoulos**[2,4], **A. Laaksonen**[5,6], **N. M. Donahue**[1], **and S. N. Pandis**[1,2]

[1]Center for Atmospheric Particle Studies, Carnegie Mellon University, Pittsburgh, PA, USA
[2]Institute of Chemical Engineering and High Temperature Chemical Processes (ICE-HT), Foundation of Research and Technology (FORTH), Patra, Greece
[3]Laboratory of Atmospheric Chemistry, Paul Scherrer Institut, Villigen, Switzerland
[4]Environmental Chemical Processes Laboratory (ECPL), University of Crete, Heraklion, Greece
[5]Department of Applied Physics, University of Eastern Finland, Kuopio, Finland
[6]Finnish Meteorological Institute, Helsinki, Finland

Received: 26 May 2011 – Accepted: 14 June 2011 – Published: 11 July 2011

Correspondence to: S. N. Pandis (spyros@andrew.cmu.edu)

Published by Copernicus Publications on behalf of the European Geosciences Union.

Abstract

Atmospheric particles were measured in the winter at a remote coastal site on the island of Crete, Greece during the Finokalia Aerosol Measurement Experiment-2009. A Quadrupole aerosol mass spectrometer (Q-AMS) was employed to quantify the size-resolved chemical composition of non-refractory submicron aerosol, and a thermodenuder was used to analyze the organic aerosol (OA) volatility. Complementary measurements included particle size distributions from a scanning mobility particle sizer, inorganic and organic particle composition from filter analysis, concentrations of O_3, NO_x and NO_y, and meteorological measurements. Factor analysis was performed on the OA mass spectra, and the variability in OA composition could best be explained with three OA components. The oxygenated organic aerosol (OOA) was similar in composition and volatility to the summertime OA previously measured at this site and appears to represent an effective endpoint in particle-phase oxidation of organics. The two other OA components, one associated with amines (Amine-OA) and the other probably associated with the burning of olive branches (OB-OA), had lower volatility but were less oxygenated. Hydrocarbon-like organic aerosol (HOA) was not detected. The absence of OB-OA and Amine-OA in the summer data may be due to lower emissions and/or photochemical conversion of these components to OOA.

1 Introduction

Submicrometer atmospheric particles adversely affect human health (Davidson et al., 2005; Pope and Dockery, 2006) and regional visibility (Watson, 2002), and they have a highly uncertain effect on climate (IPCC, 2007). Organic aerosol (OA) constitutes a significant fraction of the submicron particle mass (Kanakidou et al., 2000; Zhang et al., 2007). Understanding the formation and concentrations of OA is challenging because OA has a myriad sources, its formation involves complex and poorly understood chemistry, and it is highly dynamic. After its initial formation, OA can partition between the gas and particle phases (Pankow, 1994) and can be further processed in either phase (Kalberer et al., 2004; Robinson et al., 2006; Hallquist et al., 2009). While much progress has been made in identifying and understanding these processes (Robinson et al., 2007; Hallquist et al., 2009; Jimenez et al., 2009; Ng et al., 2010), significant gaps remain in our understanding of the formation and transformation of OA in the atmosphere.

Recently, factor analysis of OA mass spectra from Aerosol Mass Spectrometer (AMS) data has enabled separation of OA based on composition (Ulbrich et al., 2009). The results have been used to make inferences about the sources and transformation of OA in the atmosphere (Lanz et al., 2007, 2008; Hildebrandt et al., 2010a; Ulbrich et al., 2009; Morgan et al., 2010; Ng et al., 2010). At most locations, the OA can be separated into two main components: hydrocarbon-like organic aerosol (HOA), a reduced component associated with fresh emissions, and oxygenated organic aerosol (OOA), a more oxidized component associated with OA that has been processed in the atmosphere (Zhang et al., 2007; Ng et al., 2010). Most OA in the atmosphere is usually OOA (Zhang et al., 2007; Lanz et al., 2010; Morgan et al., 2010), and hence it is especially important to understand the formation of this OA component.

The Finokalia station is an excellent location to study oxidized OA since it is isolated and therefore far from typical fresh OA sources (traffic, meat cooking, etc.). We conducted two campaigns at this site to measure OA under different photochemical conditions in the early summer (FAME-08, 8 May–5 June 2008) and the late winter (FAME-09, 25 February–26 March 2009). Factor analysis of the FAME-08 OA resulted in two OOA components with different extents of oxidation but similar volatility (Hildebrandt et al., 2010a). These OOA components do not appear to correspond to different OA sources but instead to different limits of the extent of OA oxidation observed during the campaign (Hildebrandt et al., 2010a). Wintertime OA sampled during FAME-09 was less oxygenated and more variable in composition than summertime OA sampled during FAME-08 (Hildebrandt et al., 2010b). The differences in OA composition during the two campaigns are associated with differences in the photochemical conditions

(Hildebrandt et al., 2010b). However, the bulk OA analysis does not reveal whether the FAME-09 OA was composed of less oxygenated OOA or whether it was composed of highly oxygenated OOA in addition to fresher OA components. In this manuscript we explore in more detail the composition and sources of the wintertime OA using AMS factor analysis on the organic aerosol mass spectra. We interpret the results in the context of meteorological conditions at the site and other measurements taken during the campaign, including measurements of fine and coarse particle composition from filters, aerosol size distributions and OA volatility. Our results provide insights into the sources and atmospheric processing of organic aerosol.

2 Experimental

The Finokalia Aerosol Measurement Experiment – 2009 (FAME-09) was conducted from 25 February–26 March 2009 at the Finokalia Station of the Environmental Chemical Processes Laboratory of the University of Crete (Mihalopoulos et al., 1997) as part of the EUCAARI intensive winter campaign (Kulmala et al., 2009).

2.1 Instrumentation

The size-resolved submicron aerosol composition was measured using a Quadrupole Aerosol Mass Spectrometer (Q-AMS) from Aerodyne Research, Inc. (Canagaratna et al., 2007). Here we focus on the organic aerosol mass spectra, which are derived from the total aerosol mass spectra using the standard fragmentation table (Allan et al., 2004) with a few modifications, as described in the auxiliary material of Hildebrandt et al. (2010b). The particle size distribution was monitored using a scanning mobility particle sizer (SMPS, TSI classifier model 3080, CPC 3772 or 3776). The volatility of OA was analyzed using a thermodenuder (TD) system (Lee et al., 2010). In brief, aerosol passed alternately through the TD, heated to a predefined temperature, or a bypass line. The aerosol was sent through the same sampling line to the SMPS for online measurements of the particle size distribution and to the Q-AMS for measurements of the particle chemical composition. The volatility of the OA was determined by comparing the residual aerosol after the TD to the ambient aerosol that was passed through the bypass line.

Daily PM_1 (particulate matter smaller than 1 µm in diameter) and PM_{1-10} (larger than 1 µm but smaller than 10 µm in diameter) filter samples were collected using a virtual impactor (Loo, 1988). For the analysis of inorganic ions, filters were extracted with nanopure water and water-soluble ions were measured by conductivity detectors (Koulouri et al., 2008; Pikridas et al., 2010). Carbonaceous material was analyzed from PM_1 collected daily on quartz fiber filters. Elemental and organic carbon (EC and OC) were determined from these filters using a carbon analyzer (Sunset Laboratory Inc., Oregon) and a modification of the NIOSH thermal-optical transmission method (Koulouri et al., 2008; Pikridas et al., 2010). A number of other measurements were performed during this campaign, including aerosol light scattering and absorption, concentrations of O_3, NO_x and NO_y, and meteorological measurements (temperature, relative humidity and radiation intensity).

2.2 Methods

We categorized the air masses based on their source region using the potential emission sensitivity values (PES) of the footprint residence time plots from the FLEXPART model (Stohl et al., 1998) as described by Pikridas et al. (2010). The resulting categories, named by the region which appeared to have the major influence on the air mass composition, are: Africa, Athens, Crete, Greece (after excluding Athens and Crete), marine and other continental. Athens, Crete and Greece were separated from other continental regions in order to investigate whether it is possible to detect the signature of local sources (Crete) or regional sources (Athens, Greece) at the field site. Figure 1 shows the categorized source regions for the site throughout the campaign. The most abundant source category during FAME-09 was Crete (50 %), the second most abundant was marine (15 %), and the least abundant was Africa (6 %). It is often not clear whether the major influence was marine, Crete or Africa. As a result, the dust storm period (7–9 March) when PM_{10} concentrations were high is in the Crete category, whereas PM_{10} concentrations were low in the Africa category.

We applied positive matrix factorization (PMF) to the time series of the organic aerosol mass spectra from the Q-AMS, using the PMF2 algorithm (version 4.2) by P. Paatero to solve the bilinear unmixing problem (Paatero and Tapper, 1994). We examined different PMF solutions (varying the number of factors and other PMF settings) and evaluated them with respect to ancillary data (data not included in the PMF analysis, e.g. sulfate measurements) and mathematical diagnostics, as described in more detail in the Appendix. In order to examine whether the OA factors exhibited statistically significant diurnal variation, we conducted one-way analysis of variance (ANOVA) tests with factor concentrations and total OA as dependent variables and time of day as the independent variable (Hildebrandt et al., 2010a). Before conducting ANOVA, we removed the data points when the aerosol was clearly influenced by fire plumes (7, 24 and 26 March) so that OA spikes associated with the fire plumes do not mask the diurnal cycle.

Analyzing OA volatility using thermodenuder data

The AMS collection efficiency (CE) was estimated for the ambient aerosol and the thermodenuded aerosol using the algorithm of Kostenidou et al. (2007), as in our previous study (Lee et al., 2010), to account for potential changes in the CE upon heating and evaporating part of the particle mass. The CE of the ambient aerosol ranged from 0.5 to 0.85 (average = 0.6), the CE of the thermodenuded OA ranged from 0.4 to 0.75 (average = 0.6), and we applied the estimated time-dependent CE to all data. The lower CE during FAME-09 compared to FAME-08 may be due to differences in aerosol composition or to the fact that different Q-AMS instruments were used for these two campaigns. The TD data were also corrected for particle losses in the TD, which depend on particle size, thermodenuder temperature and residence time, and which were determined in calibration experiments (Lee, 2010). During six days of the campaign

(6–12 March), SMPS data were not available, and the CE and particle losses could not be estimated for this time period. We do not use the data from these days to analyze the OA volatility. We do use the data for ambient OA analysis after correcting the data with the campaign-average ambient CE.

The concentrations of the OA factors were often low and close to the detection limit of the AMS. For the TD analysis, we therefore eliminated all data points when the ambient factor concentrations were below 0.2 $\mu g\, m^{-3}$, a reasonable estimate for the detection limit of the Q-AMS (Drewnick et al., 2009). We analyzed the volatility of the different OA components by first computing their mass fraction remaining (MFR, the ratio of the thermodenuded organic mass to the ambient organic mass). We kept the thermodenuder at a temperature of approximately 100 °C for most of FAME-09 to be able to observe changes in the OA volatility over the course of the campaign. We also varied the TD temperature during some parts of the campaign to be able to construct thermograms (MFR as a function of TD temperature) of the OA (Lee et al., 2010). We can use these data and the organic aerosol evaporation model (Lee et al., 2010; Riipinen et al., 2010) to estimate the OA volatility. Considering the large uncertainty in estimating OA volatility distributions (Lee et al., 2010) we here limit the analysis to comparing the volatility of the FAME-09 OA to the volatility of the FAME-08 OA (Hildebrandt et al., 2010a).

The base-case volatility basis set used to estimate the FAME-08 OA volatility consisted of four saturation mass concentrations (C^*) of 0.01, 0.1 1 and 10 $\mu g\, m^{-3}$, abbreviated as [0.01 0.1 1 10]; the corresponding mass fraction values were estimated as [0.2 0.2 0.3 0.3] (Lee et al., 2010). In order to compare this volatility to the FAME-09 OA volatility, we use the aerosol evaporation model with the same effective mass accommodation coefficient and vaporization enthalpy as for the FAME-08 base case (0.05 and 80 $kJ\, mol^{-1}$, respectively). We set the volatility basis set as $s \times [0.01\ 0.1\ 1\ 10]$ where s is a multiplicative "shifting factor" from the FAME-08 volatility basis set. We fix the mass fraction values to the values estimated for FAME-08 and use the evaporation model to calculate the shifting factor while minimizing the residuals between measured and modeled MFR. The evaporation model accounts for differences between the two campaigns in OA concentrations, particle size distributions and thermodenuder residence times. Thus, the analysis conducted here is more rigorous and more accurate than a comparison of thermograms collected during the two campaigns, given the differences in concentrations, particle size distributions and residence times.

3 Results and discussion

3.1 Filter measurements and meteorological conditions

A summary of the filter measurements is presented in Fig. 2 for fine PM (PM_1, panel a) and coarse PM (PM_{1-10}, panel b). During 7–9 March, the area experienced a dust storm resulting in PM_{10} concentrations exceeding 500 µg m^{-3} at times (data from an Aerodynamic Particle Sizer, not shown). Outside of the dust-storm period, fine PM was usually dominated by ammonium, sulfate, and organics, consistent with the AMS data during this time period (Hildebrandt et al., 2010b) and also with previous studies at Finokalia (Koulouri et al., 2008; Pikridas et al., 2010). Organic mass from the filter samples was estimated by multiplying filter measurements of organic carbon by the ratio of organic mass to organic carbon (OM : OC) estimated from AMS measurements using the correlations developed by Aiken et al. (2008). The campaign-average estimated OM : OC ratio was 1.8; daily averages ranged from 1.6 to 1.9. Q-AMS measurements of organic mass agreed well with filter measurements (slope = 1.0, $R^2 = 0.79$); Q-AMS measurements of sulfate mass agreed reasonably well with measurements from filters (slope = 0.68, $R^2 = 0.62$). It is possible that this slope is less than 1 because of the lower size cutoff of the AMS and the significant sulfate concentrations above ∼ 0.7 µm (Hildebrandt et al., 2010b). Sulfate concentrations attributable to sea salt (which is not detected by the Q-AMS) were only 0.05 µg m^{-3} on average and therefore do not affect the slope significantly. Measured Na^+ concentrations correlated well with Cl^- ($R^2 = 0.73$), suggesting a common origin (sea salt). Thus, sea salt concentrations were approximated based on sea water composition and the measured concentrations of Na^+, Cl^-, Mg^{2+}, K^+, Ca^{2+} and SO_4^{2-} as in previous work (Sciare et al., 2005). Dust concentrations in the fine and coarse mode were not measured explicitly but were estimated as the sum of the non-speciated PM and Ca^{2+} not attributed to sea salt.

The coarse-mode composition was dominated by dust, sea salt and nitrate. Measured concentrations of Na^+ correlated well with Mg^{2+} ($R^2 = 0.89$) and with Cl^- ($R^2 = 0.91$), confirming a common origin (sea salt), and PM_{1-10} sea salt concentrations were approximated according to Sciare et al. (2005). The average Cl^-/Na^+ mass ratio was equal to 1.45, a bit lower than the typical ratio of 1.8 reported for sea water (Seinfeld and Pandis, 2006). Lower Cl^-/Na^+ mass ratios have been observed in previous studies at this site (Sciare et al., 2005; Pikridas et al., 2010), and they are due to reactions of nitric and sulfuric acid with NaCl and subsequent release of HCl.

The ratio of organic carbon to elemental carbon (OC : EC) in fine PM can be an indicator of photochemical activity during the campaign (Cabada et al., 2004). The OC : EC slope of 2.6 (Fig. 3), obtained from filter measurements, suggests moderate photochemical activity during this campaign – much less than during the summer when the OC : EC slope was 5.4 (Pikridas et al., 2010). This is consistent with the analysis of the AMS mass spectra, which indicated significantly less oxidized organic aerosol during FAME-09 (Hildebrandt et al., 2010b). During the dust storm the OC : EC ratio is lower, consistent with less atmospheric processing or fresher emissions. This was also observed during the summer campaign (Pikridas et al., 2010) and is attributed to the influence of major cities in Africa or interference of crustal elements in the EC analysis.

We used meteorological measurements taken at the site and data from the European Centre for Medium-Range Weather Forecasts (www.ecmwf.int/research/era/do/get/era-interim) to evaluate the photochemical conditions at the site. The conditions were significantly different during the first few days of the campaign (25–28 February) compared to the campaign-average conditions. The average solar radiation measured at the site was lower during those days: $75\,W\,m^{-2}$ compared to the campaign-average of $175\,Wm^{-2}$. According to the ECMWF, the average low cloud cover in the grid cell containing the site (see Fig. S1 in Hildebrandt et al., 2010b) was 0.56 from 25–28 February, compared to the campaign-average of 0.16. This difference in photochemical conditions presents a unique opportunity to evaluate the effect of photochemistry on aerosol composition. The relative humidity was also higher during the first few days – the 25–28 February average was 82 % compared to the campaign-average of 73 %.

3.2 Aerosol size distribution

During FAME-09, the aerosol size distribution was more variable than during the summer campaign (Pikridas et al., 2010), primarily due to the higher frequency of nucleation events during FAME-09 (Pikridas et al., 2011) and the more variable meteorological conditions. Figure 4 shows the campaign-average number and volume size distributions for FAME-09. The average number size distribution for FAME-09 was bimodal with the dominant mode located at 50 nm, differently from FAME-08 when the number size distribution only had one mode located at 90 nm (Pikridas et al., 2010). The volume distribution during FAME-09 was centered at 230 nm, compared to 300 nm during FAME-08 (Pikridas et al., 2010).

The FAME-09 time series of total particle concentrations from the SMPS (particle mobility diameter 15–500 nm) and the concentration of particles smaller than 30 nm in diameter are shown in Fig. 5. The figure also indicates the times when nucleation events were identified based on the increase in total concentrations of air ions with diameters between 2 nm and 10 nm (Pikridas et al., 2011), and when small agricultural fires were observed from the field site. Nucleation events are clearly distinguishable from the influence of fires; while nucleation events resulted in an increase in mostly small particles (15 nm $< D_\mathrm{p} <$ 30 nm) which lasted for several hours, the influence of the fires was usually in the form of a spike in total particle number, not in the number of small particles. This suggests that even though the fires associated with these spikes were local, the particles coagulated, grew or even evaporated quickly after emission. The delay between the nucleation events identified based on increases in air ion concentrations (2–10 nm) and the increase in particle concentrations from the SMPS (> 15 nm) is caused by the growth of the particles to the SMPS size range.

3.3 Results and interpretation of Positive Matrix Factorization (PMF) analysis

We here focus on the 3-factor PMF solution, which best represents our data as explained in the Appendix. The time series and mass spectra of the three factors (OA components) are presented in Figs. 6 and 7, respectively. The first factor is dominated by fragments at a mass-to-charge (*m/z*) ratio of 58 and also has a significant (but much smaller) contribution at *m/z* 86. These fragments are likely due to amide functional groups (Takami et al., 2005), consistent with speciation studies at Finokalia which reveal the presence of amines there (Violaki and Mihalopoulos, 2010). We therefore name the first factor Amine-OA. Spikes in the concentrations of the second factor were associated with the observation of small fires close to the measurement site (Fig. 7b), most likely the private burning of olive branches, which is common at this time of the year throughout Greece and the Balkans. However, the profile of the factor does not resemble biomass burning organic aerosol, BBOA (Ng et al., 2011), and we therefore name this factor OB-OA (Olive branch – OA) to avoid confusion with more typically observed BBOA. The third PMF factor resembles oxygenated organic aerosol (OOA), a factor extracted in all PMF analysis (Ng et al., 2011) and typically associated with OA that has been processed in the atmosphere. We note that the spikes likely associated with the burning of olive branches are also visible in the concentrations of OOA, suggesting that the OB-OA can be rapidly converted to OOA. The average concentrations of these factors and their contribution to total OA in air masses from the different source regions are summarized in Table 1. The OOA factor always accounts for more than 50 % of the OA mass, while the OB-OA factor usually accounts for most of the rest. Correlations of the factor time series with ancillary data are summarized in Table A2 and discussed in more detail in Sects. 3.3.1–3.3.3 below.

The concentrations of total OA, OOA and OB-OA exhibited statistically significant diurnal variation ($p = 0.007$, 0.02, 0.007, respectively), and the diurnal cycles of their average concentrations are presented in Fig. 8, along with the diurnal cycle of the average ozone concentration. We split the Amine-OA data into two periods: the first week (until noon on 3 March) and the rest of the campaign. The Amine-OA concentrations were much higher during the first week and did not exhibit statistically significant diurnal variation ($p = 0.42$). During 3–26 March, Amine-OA concentrations were very low, but they did exhibit statistically significant diurnal variation ($p = 1 \times 10^{-5}$, Fig. 8). The diurnal cycle of the different OA factors is discussed in more detail in the following sections.

3.3.1 Amine-OA

Amine-OA was not detected elsewhere in Europe during the EUCAARI intensive periods (Prevot et al., 2011). While the signal of amine functional groups can be enhanced in the AMS due to surface ionization, we did not observe this effect (Hildebrandt et al., 2010b). Figure 9 shows the Amine-OA concentrations during the first week of FAME-09, colored by source region, as well as total aerosol number concentrations from the SMPS. The Amine-OA concentration is not correlated to total particle number ($R^2 = 0.00$, Table A2). Hence, the Amine-OA is likely not associated with local or regional combustion sources, as further confirmed by the lack of significant correlations between the Amine-OA and typical fresh combustion tracers such as EC and NO_x (CO measurements were not available for this campaign). The Amine-OA also does not seem to be linked with sea salt since the filter measurements (Fig. 2) suggest that sea salt concentrations were not higher during the first week compared to the rest of the campaign.

When averaging over the entire campaign, Amine-OA concentrations were higher from Greece and the “other continental” source region than from Africa or the marine source region (Table 1). However, this does not necessarily imply that the Amine-OA is associated with Greece, for example, as the concentrations were much lower when the air originated from Greece later in the campaign. Instead, the higher Amine-OA concentrations appear to be associated with the milder photochemical conditions during the first few days of the campaign when cloud cover at the site was higher and solar radiation was lower (Sect. 3.1). There was also a significant contribution from the Amine-OA during 1–4 March when solar radiation measured at the site was much higher (average 211 $\mathrm{W m^{-2}}$). However, during 1–4 March the Amine-OA concentrations peak during the night (Fig. 9), consistent with the Amine-OA concentrations being associated with dearth of solar radiation and/or abundance of clouds. Plausible explanations for our observations include that the cloudy and nighttime conditions prevent the quick and efficient degradation of Amine-OA by photochemical oxidation, and/or that the presence of Amine-OA is associated with cloud processing.

This is consistent with our observations during FAME-08 when under very high photochemical activity no Amine-OA factor was detected at the same location (Hildebrandt et al., 2010a). We obtain a measure of the Amine-OA volatility by averaging its MFR at a thermodenuder residence time of 30 s over temperatures of 85–115 °C, at which most of the data were collected. The average MFR is 1 (Amine-OA did not evaporate significantly in our thermodenuder), suggesting that the Amine-OA has very low volatility. This is consistent with the findings of recent laboratory experiments (Smith et al., 2010).

3.3.2 OB-OA

The OB-OA is characterized by high contributions from *m/z* 27, 29, 43, 55, 85 and 87, as well as significant contributions at high *m/z* (46 % of the organic mass at $m/z > 120$), which is not typically observed in AMS spectra of ambient OA. The OB-OA mass spectrum does not resemble the mass spectra of humic or fulvic acid (Alfarra, 2004) and therefore likely does not represent a humic-like substance. Even though the diurnal variation of the OB-OA is statistically significant (Fig. 8), the variation is small, and we do not expect to be able to explain it with meteorological or photochemical conditions considering that the factor appears to be associated with the burning of olive tree branches.

Potassium emissions are often associated with biomass-related fires. Here we use the AMS signal at *m/z* 39 as a proxy for potassium and therefore a tracer of fires. This assumes that the signal of $C_3H_3^+$ is negligible, a reasonable assumption considering the high total signal at *m/z* 39 ($\sim 50\,\mu g\,m^{-3}$ on average). The signal of potassium is enhanced in the AMS due to surface ionization and hence the absolute AMS-potassium measurements are not trustable; however, the relative values are still informative. We find a strong correlation between the concentrations of OB-OA and AMS-potassium ($R^2 = 0.57$), further confirming that this OA is associated with fires. The OB-OA is also significantly correlated with EC concentrations ($R^2 = 0.28$) as expected for incomplete combustion emissions.

The fires influencing the observed OA are not necessarily local. Figure 10 shows a time series of OB-OA for the first 8 days of the campaign, colored by source region, and the time series of total particle number from the SMPS. OB-OA concentrations can be relatively high for essentially all source regions. For example, on 28 February OB-OA concentrations were elevated when the air mass originated from Athens and Greece. The OB-OA on 4 March might be due to fires on Crete; however, they are likely not local fires since the increase in OB-OA was not associated with an increase in particle number. While the local fires are reflected by spikes in the OB-OA, the regional fires are represented by longer periods of elevated OB-OA concentrations. Similarly to the Amine-OA, the OB-OA did not evaporate significantly in our thermodenuder. At a thermodenuder residence time of 40 s, the mass fraction remaining of the OB-OA averaged over all data at TD temperatures ranging from 85 °C to 115 °C was 1. There was no significant difference in the mass fraction remaining for the different periods in Fig. 10. The signal at *m/z* 85 and *m/z* 87 (Fig. 6) may be due to amine functional groups; hence, the low volatility of the OB-OA may be associated with the stabilizing effects of amines (Smith et al., 2010).

The OB-OA mass spectrum also has significant contributions from ions at *m/z* 55 and 57, fragments typically associated with HOA. However, the contributions of *m/z* 55 and 57 appear to be due to organic fragments associated with fires, not due to a hidden

HOA factor, as explained in more detail in the Appendix. Methods to estimate the contribution of HOA (Ng et al., 2011) result in average values between $-0.07\,\mu\text{g m}^{-3}$ and $-0.03\,\mu\text{g m}^{-3}$, suggesting that HOA concentrations were very low and that the estimation methods may not be appropriate at these very low concentrations. Thus, just like during the summer campaign (Hildebrandt et al., 2010a), HOA was not present in significant amounts during FAME-09. A plausible explanation for the lack of observed HOA during this study is evaporation: while HOA has been shown to exhibit significant volatility (Robinson et al., 2007; Huffman et al., 2009), the Amine-OA and OB-OA observed here are practically non-volatile within the error of our measurements. Thus, HOA may evaporate by the time it reaches the site while OB-OA and Amine-OA do not.

3.3.3 OOA

OOA was the most abundant factor, as expected for a remote site. The diurnal cycle of OOA is similar to that of total OA and ozone and can be explained by meteorology and photochemical conditions: concentrations were lowest in the early morning, peaked in the early afternoon and then decreased slightly before rising again in the evening. The peak in the early afternoon is most likely associated with photo-oxidation. The rise in the evening may be associated with changes in the boundary layer height. Highly oxidized OOA (also referred to as OOA-1 or LV-OOA) is typically highly correlated with sulfate (SO_4^{2-}) concentrations (Lanz et al., 2007; Ulbrich et al., 2009; Hildebrandt et al., 2010a), and less oxidized OOA (also referred to as OOA-2 or SV-OOA) is typically correlated with nitrate (NO_3^-) concentrations (Lanz et al., 2007; Ulbrich et al., 2009). The OOA measured here is highly correlated with SO_4^{2-} ($R^2 = 0.54$) and NH_4^+ ($R^2 = 0.58$); concentrations of NO_3^- in PM_1 were very low throughout the campaign.

The OOA is the only component of the OA sampled during FAME-09 that exhibited a semi-volatile nature. Figure 11 shows four OOA thermograms obtained during different times of the campaign when we varied the TD temperature to investigate OA volatility. We use these data to calculate the shifting factor relative to the FAME-08 OA

Title Page
Abstract | Introduction
Conclusions | References
Tables | Figures
◀| |▶
◀ ▶
Back | Close
Full Screen / Esc
Printer-friendly Version
Interactive Discussion

volatility as explained in Sect. 2.2. The calculated shifting factor is 1.0 – the volatility of OOA during FAME-09 is the same as the volatility of OA (entirely OOA) during FAME-08. Furthermore, the mass spectrum of the FAME-09 OOA is similar to the mass spectrum of the FAME-08 OOA. We here summarize the mass spectrum with f_{43} and f_{44} (the fraction of total OA mass due to fragments at *m/z* 43 and *m/z* 44, respectively) which are used to characterize the extent of oxidation of OOA (Ng et al., 2010). In the FAME-09 OOA, f_{43} was 4.6 % and f_{44} was 16.9 %. In the FAME-08 OA, one of the OOA components exhibited $f_{43} = 6.5\,\%$ and $f_{44} = 13.1\,\%$; the other OOA component exhibited $f_{43} = 4.5\,\%$ and $f_{44} = 21.7\,\%$. Thus, the extent of oxidation of the FAME-09 OOA was in between the extents of oxidation of the two OOA factors extracted from the FAME-08 OA, and it was very similar to the average extent of oxidation of the FAME-08 OA ($f_{43} = 5.3\,\%$ and $f_{44} = 18.2\,\%$). Overall, the OOA observed in the winter is similar to the OOA observed in the summer in terms of both volatility and extent of oxidation.

4 Conclusions

We sampled organic aerosol (OA) at Finokalia during the late winter (FAME-09) when oxidizing conditions were milder than during the early summer (FAME-08). Results from filter analysis are consistent with bulk aerosol mass spectrometer data and suggest that the OA was less oxidized in the winter than in the summer. Factor analysis on the OA mass spectra revealed that the OA sampled at Finokalia was entirely composed of OOA during the summer. Under milder oxidizing conditions in the winter, the OA is composed of similar OOA mixed with fresher OA components – one component probably associated with the burning of olive branches and a second component associated with amines. The most traditional primary OA component HOA was still entirely absent in the winter. This is presumably because the HOA, as opposed to OB-OA and Amine-OA, is semi-volatile and therefore evaporates and is oxidized to OOA before reaching the site.

Considering that the wintertime OOA sampled during FAME-09 exhibited a similar extent of oxidation as the summertime OOA sampled during FAME-08, it appears that the OOA at Finokalia represents an effective end-point in the oxidation of particle-phase organics. Differences in the extent of oxidation of the bulk OA occur when fresher OA components are mixed with this OOA. The fresher OA components appear to age toward OOA under the harsher oxidizing conditions in the summer.

Appendix A

Positive Matrix Factorization (PMF) analysis

A1 General remarks

The bilinear unmixing problem solved in PMF analysis is represented in matrix form by:

$$\mathbf{X} = \mathbf{G}\mathbf{F} + \mathbf{E} \tag{A1}$$

where **X** is an $m \times n$ matrix of the measured data with m rows of average mass spectra (number of time periods $= m$) and n columns of time series of each *m/z* sampled (number of *m/z* fit $= n$). **F** is a $p \times n$ matrix with p factor profiles (constant mass spectra), **G** is an $m \times p$ matrix with the corresponding factor contributions, and **E** is the $m\times\ n$ matrix of residuals. **G** and **F** are fit to minimize the sum of the squared and uncertainty-scaled residuals (Paatero and Tapper, 1994).

Different PMF solutions can be obtained by varying the PMF settings, model parameters, and the input matrix, **X**. We have found previously that the PMF solutions are mostly sensitive to the number of factors, p, chosen, and to the rotations induced by the f_{peak}-parameter (Hildebrandt et al., 2010a). Thus, we focus on choosing the number of factors and the rotation in the sections below. The other settings were similar as for the analysis of the FAME-08 dataset. We did not add modeling uncertainty to the instrumental uncertainty, we used the default convergence criteria, and we used the most highly resolved data (3 min averages) for the PMF analysis and then performed further averaging in post-analysis of the data. We used the entire organic data matrix **X** (*m/z*'s 12…300), but excluded the contributions at *m/z* 39 and 41 as these signals were influenced by a high potassium signal (Hildebrandt et al., 2010b). We generally did not exclude OA plumes from the data matrix **X** except for one period (~ 14:30 on 22 March) when an OA plume associated with fires resulted in OA concentrations exceeding 500 µg m^{-3}. PMF analysis on the complete dataset (including thermodenuded and ambient data) and on the ambient only data yielded similar results. The factor time series and mass presented in this manuscript are from the analysis on the ambient only data. Finally, we chose different pseudo-random starting values for the algorithm in PMF2 (i.e. we changed the "seed"-numbers), but did not observe significant changes in our results.

A2 Number of factors (*p*)

First, we investigated the choice of different numbers of factors, *p*, with respect to ancillary data. The 1-factor PMF solution yielded a spectrum with significant contributions from *m/z* 44 and *m/z* 58 which does not resemble mass spectra previously extracted from PMF analysis. The 2-factor solution resulted in one factor resembling OOA, and the corresponding time series correlated with sulfate and ammonium measured by the AMS (Table A1). The second factor in the 2-factor solution is dominated by ions at *m/z* 58 and also has significant contributions at *m/z* > 100 amu. This factor correlated weakly with fresh emission tracers (EC, NO$_x$, potassium, Table A1). The 3-factor solution yielded "OOA", the time series of which correlated more strongly with sulfate and ammonium than the "OOA" in the 2-factor solution (Table A2). The 3-factor solution also yielded a factor with a spectrum dominated by *m/z* 58, which does not exhibit significant correlations with fresh emissions but, as noted in the text, may be associated with photochemical activity. The third factor in the 3-factor PMF solution has the largest contribution at *m/z* 85 and also has large contributions at *m/z* (46 % of the mass is due to ions at *m/z* > 120). This factor was strongly correlated with potassium measurements

(Table A2), and the time series of this factor spiked when fires were observed from the field site (Fig. 7). Thus, we attribute this factor to fires, more specifically, the burning of olive branches (OB-OA).

In moving from the 3-factor to the 4-factor solution, the first and second factors ("OOA" and "Amine-OA") do not change much, but the correlation of "OOA" with sulfate and ammonium becomes a bit weaker (Table A3). The "OB-OA" in the 3-factor solution is split into two factors (factors 3 and 4 in Table A3), one dominated by ions at *m/z* 29 (factor 3), the other dominated by ions at *m/z* 82 with additional significant contributions at *m/z* 55 and *m/z* 57 (factor 4). Factor 3 has no significant correlations, and factor 4 strongly correlates with potassium and also with EC. Hence, factor 4 is most likely attributable to fires and not the "HOA" typically extracted from PMF analysis. Overall, the distinction between factors 3 and 4, and their interpretation, is ambiguous.

In addition to the ancillary data, we also evaluated mathematical diagnostics. The sum of the squared, uncertainty-weighted residuals relative to its expected values Q/Q_{exp} decreased by 20 % from $p = 1$ to $p = 2$, by 8 % from $p = 2$ to $p = 3$, and by 5 % from $p = 3$ to $p = 4$. We also analyzed the model residuals, $\mathbf{E}$, as a function of time. Structures in these residuals indicate that some OA processes and/or OA sources cannot be fully explained by the model. The structure in the model residuals could be markedly reduced by increasing the number of factors from $p = 1$ to $p = 2$ (Fig. A1), especially during the first week of the campaign. When further increasing the number of factors from $p = 2$ to $p = 3$ only a minor decrease in the structure of the model residuals, $\mathbf{E}$, could be observed (Fig. A2). An even smaller decrease in the structure of the model residuals was observed when increasing the number of factors to $p = 4$ (not shown). We note that some significant structure in the residual remained even at $p = 3$ and $p = 4$. This suggests that some processes and/or OA sources cannot be fully explained by this mathematical model, which is based on the assumption that the measured OA mass spectra can be separated into a number of constant components.

In summary, the physical meaning of the factors can be most clearly interpreted in the 3-factor solution, and the OOA in this solution is most strongly correlated with sulfate and ammonium. Thus, considering the ancillary data, the 3-factor solution is most appropriate. The mathematical diagnostics for choosing the number of factors are not as clear as the ancillary data. While the choice of moving from $p = 1$ to $p = 2$ is clear, the decision between $p = 3$ and $p = 4$ is less clear mathematically. However, as the $p = 3$ solution is superior based on the physical interpretation, we conclude that the $p = 3$ solution best represents our data.

A3 Inducing different rotational states (f_{peak})

In contrast to the FAME-08 data set (Hildebrandt et al., 2010b), the results of the FAME-09 PMF analysis were not very sensitive to the different rotational states (f_{peak}). At $p = 3$, Q/Q_{exp} increased by only +0.7 % from $f_{\text{peak}} = 0.0$ to $f_{\text{peak}} = -0.4$, which was the largest change in Q/Q_{exp} for the f_{peak} values investigated here. We find that positive f_{peaks} increase f_{57} (the fraction of the total organic signal due to fragments at *m/z* 57) in OB-OA (1.2 %, 1.4 %, 1.6 % at f_{peaks} −0.4, 0.0, +0.4, respectively) and also f_{60} in OB-OA (0.0 %, 0.3 %, 0.3 % at f_{peaks} −0.4, 0.0, +0.4, respectively), whereas negative f_{peaks} lower the f_{58} in Amine-OA (40.7 %, 56.4 %, 71.6 % at f_{peaks} −0.4, 0.0, +0.4, respectively). The influence of f_{peak} on the OOA mass spectrum was relatively weak (f_{44} was 15.2 %, 16.9 % and 16.6 % at f_{peaks} −0.4, 0.0, +0.4, respectively). The average factor concentrations changed only moderately for different f_{peaks}: the average OOA concentration was 0.47 µg m^{-3}, 0.49 µg m^{-3} and 0.52 µg m^{-3}, the average OB-OA was 0.19 µg m^{-3}, 0.20 µg m^{-3} and 0.19 µg m^{-3}, and the average Amine-OA concentration was 0.14 µg m^{-3}, 0.10 µg m^{-3} and 0.08 µg m^{-3} at f_{peaks} −0.4, 0 and 0.4, respectively. Thus, $f_{\text{peak}} = 0.0$, which we chose, represents a compromise based on the factor mass spectra, and the PMF solution is quite robust with respect to the factor concentrations.

Acknowledgements. We thank Ilona Riipinen for her assistance with the aerosol evaporation model. This research was supported by the FP7 Integrated Project PEGASOS (contract number 265148). Lea Hildebrandt was supported by Graduate Research Fellowships from the National Science Foundation, the EPA STAR Program, the Teresa and H. John Heinz III Foundation and John and Claire Bertucci.

References

Aiken, A. C., DeCarlo, P. F., Kroll, J. H., Worsnop, D. R., Huffman, J. A., Docherty, K., Ulbrich, I. M., Mohr, C., Kimmel, J. R., Sueper, D., Sun, Y., Zhang, Q., Trimborn, A. M., Northway, M. J., Ziemann, P. J., Canagaratna, M. R., Alfarra, M. R., Prevot, A. S. H., Dommen, J., Duplissy, J., Metzger, A., Baltensperger, U., and Jimenez, J. L.: O/C and OM/OC ratios of primary, secondary, and ambient organic aerosols with high resolution time-of-flight aerosol mass spectrometry, Environ. Sci. Technol., 42, 4478–4485, 2008.

Alfarra, M. R.: Insights into atmospheric organic aerosols using an aerosol mass spectrometer, Ph.D., Chemical Engineering, University of Manchester, Manchester, 226 pp., 2004.

Allan, J. D., Delia, A. E., Coe, H., Bower, K. N., Alfarra, M. R., Jimenez, J. L., Middlebrook, A. M., Drewnick, F., Onasch, T. B., Canagaratna, M. R., Jayne, J. T., and Worsnop, D. R.: A generalised method for the extraction of chemically resolved mass spectra from aerodyne aerosol mass spectrometer data, J. Aerosol Sci., 35, 909–922, 2004.

Cabada, J. C., Pandis, S. N., Subramanian, R., Robinson, A. L., Polidori, A., and Turpin, B.: Estimating the secondary organic aerosol contribution to $PM_{2.5}$ using the EC tracer method, Aerosol Sci. Tech., 38, 140–155, 2004.

Canagaratna, M. R., Jayne, J. T., Jimenez, J. L., Allan, J. D., Alfarra, M. R., Zhang, Q., Onasch, T. B., Drewnick, F., Coe, H., Middlebrook, A. M., Delia, A., Williams, L. R., Trimborn, A. M., Northway, M. J., DeCarlo, P. F., Kolb, C. E., Davidovits, P., and Worsnop, D. R.: Chemical and microphysical characterization of ambient aerosols with the aerodyne aerosol mass spectrometer, Mass Spectrom. Rev., 26, 185–222, 2007.

Davidson, C. I., Phalen, R. F., and Solomon, P. A.: Airborne particulate matter and human health: A review, Aerosol Sci. Tech., 39, 737–749, 2005.

Drewnick, F., Hings, S. S., Alfarra, M. R., Prevot, A. S. H., and Borrmann, S.: Aerosol quantification with the Aerodyne Aerosol Mass Spectrometer: detection limits and ionizer background effects, Atmos. Meas. Tech., 2, 33–46, doi:10.5194/amt-2-33-2009, 2009.

Hallquist, M., Wenger, J. C., Baltensperger, U., Rudich, Y., Simpson, D., Claeys, M., Dommen, J., Donahue, N. M., George, C., Goldstein, A. H., Hamilton, J. F., Herrmann, H., Hoffmann, T., Iinuma, Y., Jang, M., Jenkin, M. E., Jimenez, J. L., Kiendler-Scharr, A., Maenhaut, W., McFiggans, G., Mentel, Th. F., Monod, A., Prévôt, A. S. H., Seinfeld, J. H., Surratt, J. D., Szmigielski, R., and Wildt, J.: The formation, properties and impact of secondary organic aerosol: current and emerging issues, Atmos. Chem. Phys., 9, 5155–5236, doi:10.5194/acp-9-5155-2009, 2009.

Hildebrandt, L., Engelhart, G. J., Mohr, C., Kostenidou, E., Lanz, V. A., Bougiatioti, A., DeCarlo, P. F., Prevot, A. S. H., Baltensperger, U., Mihalopoulos, N., Donahue, N. M., and Pandis, S. N.: Aged organic aerosol in the Eastern Mediterranean: the Finokalia Aerosol Measurement Experiment – 2008, Atmos. Chem. Phys., 10, 4167–4186, doi:10.5194/acp-10-4167-2010, 2010a.

Hildebrandt, L., Kostenidou, E., Mihalopoulos, N., Worsnop, D. R., Donahue, N. M., and Pandis, S. N.: Formation of highly oxygenated organic aerosol in the atmosphere: insights from the finokalia aerosol measurement experiments, Geophys. Res. Lett., 37, 2010b.

IPCC: Climate Change 2007 – The Physical Science Basis., Contribution of Working Group I to the Fourth Assessment Report of the IPCC., 2007.

Jimenez, J. L., Canagaratna, M. R., Donahue, N. M., Prevot, A. S. H., Zhang, Q., Kroll, J. H., DeCarlo, P. F., Allan, J. D., Coe, H., Ng, N. L., Aiken, A. C., Docherty, K. D., Ulbrich, I. M., Grieshop, A. P., Robinson, A. L., Duplissy, J., Smith, J. D., Wilson, K. R., Lanz, V. A., Hueglin, C., Sun, Y. L., Tian, J., Laaksonen, A., Raatikainen, T., Rautiainen, J., Vaattovaara, P., Ehn, M., Kulmala, M., Tomlinson, J. M., Collins, D. R., Cubison, M. J., Dunlea, E. J., Huffman, J. A., Onasch, T. B., Alfarra, M. R., Williams, P. I., Bower, K., Kondo, Y., Schneider, J., Drewnick, F., Borrmann, S., Weimer, S., Demerjian, K., Salcedo, D., Cottrell, L., Griffin, R., Takami, A., Miyoshi, T., Hatakeyama, S., Shimono, A., Sun, J. Y., Zhang, Y. M., Dzepina, K., Kimmel, J. R., Sueper, D., Jayne, J. T., Herndon, S. C., Trimborn, A. M., Williams, L. R., Wood, E. C., Kolb, C. E., Baltensperger, U., and Worsnop, D. R.: Evolution of organic aerosol in the atmosphere, Science, 326, 1525–1529, doi:10.1126/science.1180353, 2009.

Kalberer, M., Paulsen, D., Sax, M., Steinbacher, M., Dommen, J., Prevot, A. S. H., Fisseha, R., Weingartner, E., Frankevich, V., Zenobi, R., and Baltensperger, U.: Identification of polymers as major components of atmospheric organic aerosols, Science, 303, 1659–1662, doi:10.1126/science.1092185, 2004.

Kanakidou, M., Tsigaridis, K., Dentener, F. J., and Crutzen, P. J.: Human-activity-enhanced formation of organic aerosols by biogenic hydrocarbon oxidation, J. Geophys. Res.-Atmos., 105, 9243–9254, 2000.

Kostenidou, E., Pathak, R. K., and Pandis, S. N.: An algorithm for the calculation of secondary organic aerosol density combining AMS and SMPS data, Aerosol Sci. Tech., 41, 1002–1010, 2007.

Koulouri, E., Saarikoski, S., Theodosi, C., Markaki, Z., Gerasopoulos, E., Kouvarakis, G., Makela, T., Hillamo, R., and Mihalopoulos, N.: Chemical composition and sources of fine and coarse aerosol particles in the Eastern Mediterranean, Atmos. Environ., 42, 6542–6550, doi:10.1016/j.atmosenv.2008.04.010, 2008.

Kulmala, M., Asmi, A., Lappalainen, H. K., Carslaw, K. S., Pöschl, U., Baltensperger, U., Hov, Ø., Brenquier, J.-L., Pandis, S. N., Facchini, M. C., Hansson, H.-C., Wiedensohler, A., and O'Dowd, C. D.: Introduction: European Integrated Project on Aerosol Cloud Climate and Air Quality interactions (EUCAARI) – integrating aerosol research from nano to global scales, Atmos. Chem. Phys., 9, 2825–2841, doi:10.5194/acp-9-2825-2009, 2009.

Lanz, V. A., Alfarra, M. R., Baltensperger, U., Buchmann, B., Hueglin, C., and Prévôt, A. S. H.: Source apportionment of submicron organic aerosols at an urban site by factor analytical modelling of aerosol mass spectra, Atmos. Chem. Phys., 7, 1503–1522, doi:10.5194/acp-7-1503-2007, 2007.

Lanz, V. A., Alfarra, M. R., Baltensperger, U., Buchmann, B., Hueglin, C., Szidat, S., Wehrli, M. N., Wacker, L., Weimer, S., Caseiro, A., Puxbaum, H., and Prevot, A. S. H.: Source attribution of submicron organic aerosols during wintertime inversions by advanced factor analysis of aerosol mass spectra, Environ. Sci. Technol., 42, 214–220, 2008.

Lee, B.-H.: Volatility of atmospheric organic aerosol, Doctor of Philosophy, Chemical Engineering, Carnegie Mellon University, Pittsburgh, 155 pp., 2010.

Lee, B. H., Kostenidou, E., Hildebrandt, L., Riipinen, I., Engelhart, G. J., Mohr, C., DeCarlo, P. F., Mihalopoulos, N., Prevot, A. S. H., Baltensperger, U., and Pandis, S. N.: Measurement of the ambient organic aerosol volatility distribution: application during the Finokalia Aerosol Measurement Experiment (FAME-2008), Atmos. Chem. Phys., 10, 12149–12160, doi:10.5194/acp-10-12149-2010, 2010.

Loo, B. W. and Cork, C. P.: Development of a high efficiency virtual impactor, Aerosol Sci. Tech., 9, 167–176, 1988.

Mihalopoulos, N., Stephanou, E., Kanakidou, M., Pilitsidis, S., and Bousquet, P.: Tropospheric aerosol ionic composition in the Eastern Mediterranean region, Tellus B, 49, 314–326, 1997.

Morgan, W. T., Allan, J. D., Bower, K. N., Highwood, E. J., Liu, D., McMeeking, G. R., Northway, M. J., Williams, P. I., Krejci, R., and Coe, H.: Airborne measurements of the spatial distribution of aerosol chemical composition across Europe and evolution of the organic fraction, Atmos. Chem. Phys., 10, 4065–4083, doi:10.5194/acp-10-4065-2010, 2010.

Ng, N. L., Canagaratna, M. R., Zhang, Q., Jimenez, J. L., Tian, J., Ulbrich, I. M., Kroll, J. H., Docherty, K. S., Chhabra, P. S., Bahreini, R., Murphy, S. M., Seinfeld, J. H., Hildebrandt, L., Donahue, N. M., DeCarlo, P. F., Lanz, V. A., Prévôt, A. S. H., Dinar, E., Rudich, Y., and Worsnop, D. R.: Organic aerosol components observed in Northern Hemispheric datasets from Aerosol Mass Spectrometry, Atmos. Chem. Phys., 10, 4625–4641, doi:10.5194/acp-10-4625-2010, 2010.

Ng, N. L., Canagaratna, M. R., Jimenez, J. L., Zhang, Q., Ulbrich, I. M., and Worsnop, D. R.: Real-time methods for estimating organic component mass concentrations from aerosol mass spectrometer data, Environ. Sci. Technol., 45, 910–916, 2011.

Paatero, P. and Tapper, U.: Positive matrix factorization: a nonnegative factor model with optimal utilization of error estimates of data values, Environmetrics, 5, 111–126, 1994.

Pankow, J. F.: An absorption model of the gas/aerosol partitioning involved in the formation of secondary organic aerosol, Atmos. Environ., 28, 189–193, 1994.

Pikridas, M., Bougiatioti, A., Hildebrandt, L., Engelhart, G. J., Kostenidou, E., Mohr, C., Prévôt, A. S. H., Kouvarakis, G., Zarmpas, P., Burkhart, J. F., Lee, B.-H., Psichoudaki, M., Mihalopoulos, N., Pilinis, C., Stohl, A., Baltensperger, U., Kulmala, M., and Pandis, S. N.: The Finokalia Aerosol Measurement Experiment – 2008 (FAME-08): an overview, Atmos. Chem. Phys., 10, 6793–6806, doi:10.5194/acp-10-6793-2010, 2010.

Pikridas, M., Riipinen, I., Hildebrandt, L., Kostenidou, E., Manninen, H. E., Mihalopoulos, N., Kalivitis, N., Burkhart, J. F., Stohl, A., Kulmala, M., and Pandis, S. N.: New particle formation at a remote site in the Eastern Mediterranean, J. Geophys. Res.-Atmos., submitted, 2011.

Pope, C. A. and Dockery, D. W.: Health effects of fine particulate air pollution: lines that connect, J. Air Waste Manage., 56, 709–742, 2006.

Prevot, A. S. H., Lanz, V. A., Canonaco, F., Nemitz, E., Aijälä, M., Allan, J., Baltensperger, U., Canagaratna, M., Carbone, S., Coe, H., Dall'Osto, M., DeCarlo, P., di Marco, C., Donahue, N. M., Ehn, M., Eriksson, A., Hildebrandt, L., Hillamo, R., Freney, E., Jimenez, J.-

L., Junninen, H., Kiendler-Scharr, A., Kostenidou, E., Kulmala, M., Mensah, A., Mohr, C., Ng, S., O'Dowd, C. D., Ortega, A., Ovadnevaite, J., Pandis, S., Poulain, L., Raatikainen, T., Saarikoski, S., Sellegri, K., Sueper, D., Swietlicki, E., Tiitta, P., Ulbrich, I. M., and Worsnop, D.: Overview of organic PM_1 composition and sources in Europe (EMEP/EUCAARI campaigns in 2008–2009) determined by factor analysis of aerosol mass spectrometry (AMS) data, Atmos. Chem. Phys. Discuss., in preparation, 2011.

Riipinen, I., Pierce, J. R., Donahue, N. M., and Pandis, S. N.: Equilibration time scales of organic aerosol inside thermodenuders: Kinetic versus equilibrium thermodynamics, Atmos. Environ., 44, 597–607, 2010.

Robinson, A. L., Donahue, N. M., and Rogge, W. F.: Photochemical oxidation and changes in molecular composition of organic aerosol in the regional context, J. Geophys. Res., 11, D03302, doi:10.1029/2005JD006265, 2006.

Robinson, A. L., Donahue, N. M., Shrivastava, M. K., Weitkamp, E. A., Sage, A. M., Grieshop, A. P., Lane, T. E., Pierce, J. R., and Pandis, S. N.: Rethinking organic aerosols: semivolatile emissions and photochemical aging, Science, 315, 1259–1262, 2007.

Sciare, J., Oikonomou, K., Cachier, H., Mihalopoulos, N., Andreae, M. O., Maenhaut, W., and Sarda-Estève, R.: Aerosol mass closure and reconstruction of the light scattering coefficient over the Eastern Mediterranean Sea during the MINOS campaign, Atmos. Chem. Phys., 5, 2253–2265, doi:10.5194/acp-5-2253-2005, 2005.

Seinfeld, J. H. and Pandis, S. N.: Atmospheric Chemistry and Physics, 2nd Edn., John Wiley and Sons, Hoboken, 2006.

Smith, J. N., Barsanti, K. C., Friedli, H. R., Ehn, M., Kulmala, M., Collins, D. R., Scheckman, J. H., Williams, B. J., and McMurry, P. H.: Observations of aminium salts in atmospheric nanoparticles and possible climatic implications, P. Natl. Acad. Sci. USA, 107, 6634–6639, 2010.

Stohl, A., Hittenberger, M., and Wotawa, G.: Validation of the Lagrangian particle dispersion model FLEXPART against large scale tracer experiments, Atmos. Environ., 32, 4245–4264, 1998.

Takami, A., Miyoshi, T., Shimono, A., and Hatakeyama, S.: Chemical composition of fine aerosol measured by AMS at Fukue Island, Japan during APEX period, Atmos. Environ., 39, 4913–4924, 2005.

Ulbrich, I. M., Canagaratna, M. R., Zhang, Q., Worsnop, D. R., and Jimenez, J. L.: Interpretation of organic components from Positive Matrix Factorization of aerosol mass spectrometric data, Atmos. Chem. Phys., 9, 2891–2918, doi:10.5194/acp-9-2891-2009, 2009.

Violaki, K. and Mihalopoulos, N.: Water-soluble organic nitrogen (WSON) in size-segregated atmospheric particles over the Eastern Mediterranean, Atmos. Environ., 44, 4339–4345, 2010.

Watson, J. G.: Visibility: science and regulation, J. Air Waste Manage., 52, 628–713, 2002.

Zhang, Q., Jimenez, J. L., Canagaratna, M. R., Allan, J. D., Coe, H., Ulbrich, I., Alfarra, M. R., Takami, A., Middlebrook, A. M., Sun, Y. L., Dzepina, K., Dunlea, E., Docherty, K., DeCarlo, P. F., Salcedo, D., Onasch, T., Jayne, J. T., Miyoshi, T., Shimono, A., Hatakeyama, S., Takegawa, N., Kondo, Y., Schneider, J., Drewnick, F., Borrmann, S., Weimer, S., Demerjian, K., Williams, P., Bower, K., Bahreini, R., Cottrell, L., Griffin, R. J., Rautiainen, J., Sun, J. Y., Zhang, Y. M., and Worsnop, D. R.: Ubiquity and dominance of oxygenated species in organic aerosols in anthropogenically-influenced Northern Hemisphere midlatitudes, Geophys. Res. Lett., 34, L13801, doi:10.1029/2007gl029979, 2007.

Table 1. Contributions of OA components by source region.

	Marine ($n = 227$)	Africa ($n = 86$)	Crete ($n = 764$)	Athens ($n = 111$)	Greece ($n = 188$)	Continental, other ($n = 159$)
Amine-OA ($\mu g\,m^{-3}$)	0.05	0.05	0.07	0.18	0.17	0.16
Amine-OA/Total OA	0.06	0.07	0.11	0.14	0.18	0.21
OB-OA ($\mu g\,m^{-3}$)	0.14	0.24	0.18	0.27	0.18	0.17
OB-OA/Total OA	0.15	0.35	0.26	0.22	0.19	0.22
OOA ($\mu g\,m^{-3}$)	0.70	0.41	0.43	0.76	0.60	0.43
OOA/Total OA	0.79	0.58	0.63	0.63	0.64	0.56

Table A1. Correlations of PMF factors (f_i) with ancillary data: 2-factor PMF solution.

	$^{a}SO_4^{2-}$	$^{a}NH_4^+$	^{b}EC	NO_x	NO_y	$^{a}K^+$	$^{c}N_p$
f_1 “OOA”	0.41	0.46	0.03	0.01	0.05	0.02	0.00
f_2 “Amine”	0.05	0.07	0.21	0.01	0.24	0.21	0.06

[a] SO_4^{2-}, NH_4^+ and K^+ (potassium) measurements from AMS data.

[b] EC measurements from aethalometer data.

[c] N_p (Total particle number) measurements from SMPS data.

Table A2. Correlations of PMF factors (f_i) with ancillary data: 3-factor PMF solution.

	$^{a}SO_4^{2-}$	$^{a}NH_4^+$	^{b}EC	NO_x	NO_y	$^{a}K^+$	$^{c}N_p$
f_1 “OOA”	0.54	0.58	0.13	0.01	0.19	0.05	0.08
f_2 “Amine”	0.05	0.07	0.03	0.01	0.05	0.02	0.00
f_3 “Olive”	0.05	0.10	0.28	0.01	0.16	0.57	0.01

[a] SO_4^{2-}, NH_4^+ and K^+ (potassium) measurements from AMS data.

[b] EC measurements from aethalometer data.

[c] N_p (Total particle number) measurements from SMPS data.

Table A3. Correlations of PMF factors (f_i) with ancillary data: 4-factor PMF solution.

	$^{a}\mathrm{SO_4^{2-}}$	$^{a}\mathrm{NH_4^{+}}$	$^{b}\mathrm{EC}$	$\mathrm{NO_x}$	$\mathrm{NO_y}$	$^{a}\mathrm{K^{+}}$	$^{c}N_\mathrm{p}$
f_1 "OOA"	0.53	0.49	0.15	0.01	0.18	0.06	0.03
f_2 "Amine"	0.04	0.06	0.03	0.00	0.00	0.02	0.00
f_3 "Olive"	0.01	0.07	0.00	0.00	0.01	0.00	0.09
f_4 "HOA?"	0.04	0.08	0.28	0.00	0.15	0.59	0.01

[a] $\mathrm{SO_4^{2-}}$, $\mathrm{NH_4^{+}}$ and $\mathrm{K^{+}}$ (potassium) measurements from AMS data.

[b] EC measurements from aethalometer data.

[c] N_p (Total particle number) measurements from SMPS data.

Title Page
Abstract | Introduction
Conclusions | References
Tables | Figures
◀| |▶
◀ ▶
Back | Close
Full Screen / Esc
Printer-friendly Version
Interactive Discussion

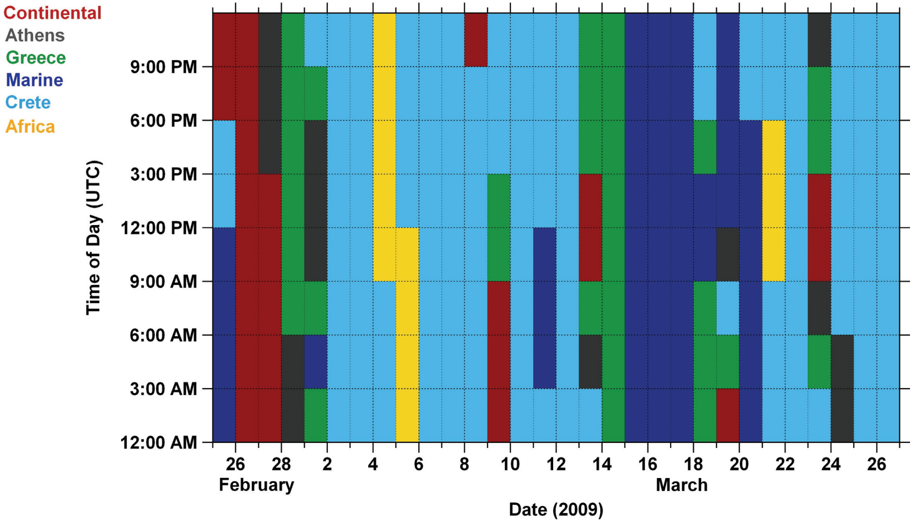

Fig. 1. Results of source region analysis based on FLEXPART footprint residence time plots (Stohl et al., 1998; Pikridas et al., 2010).

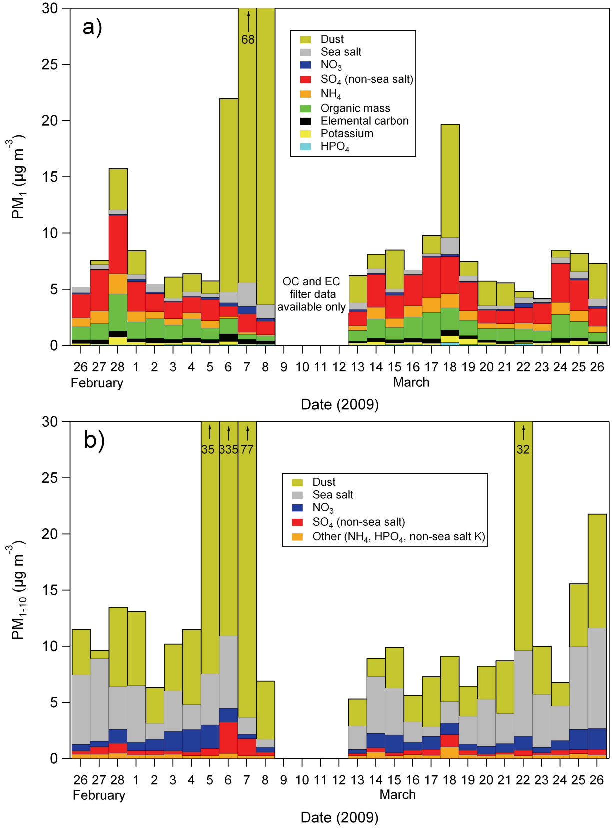

Fig. 2. Filter composition of fine PM **(a)** and coarse PM **(b)** measured during FAME-09. Fine PM is dominated by organics, sulfate and ammonium, consistent with previous work. Coarse PM is dominated by sea salt, dust and nitrate.

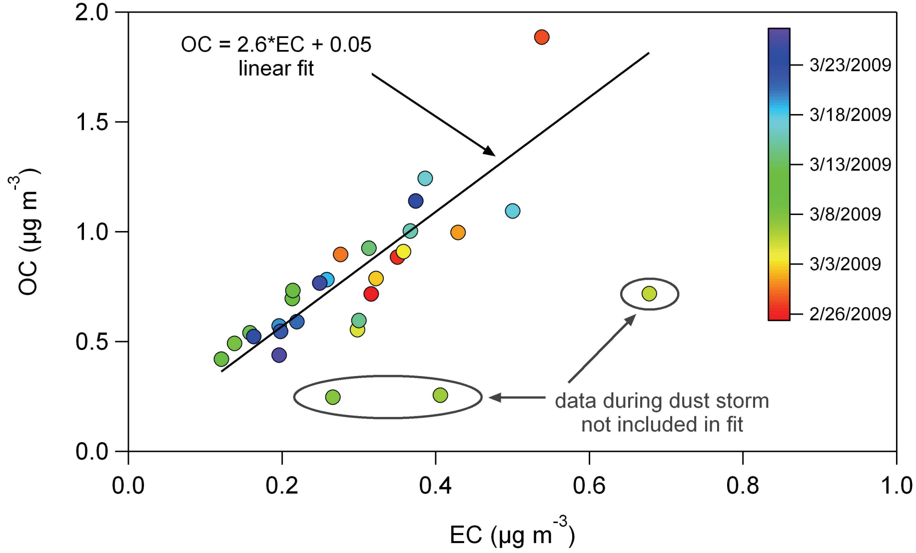

Fig. 3. Correlation of organic carbon (OC) and elemental carbon (EC) measured during the campaign for PM_1. Data points are colored by time during the campaign. The OC : EC ratio during the dust storm period was much lower than during the rest of the campaign, and these points were not included in the linear fit. Overall, the OC : EC ratio was much lower than during the summer, consistent with a moderate extent of oxidation.

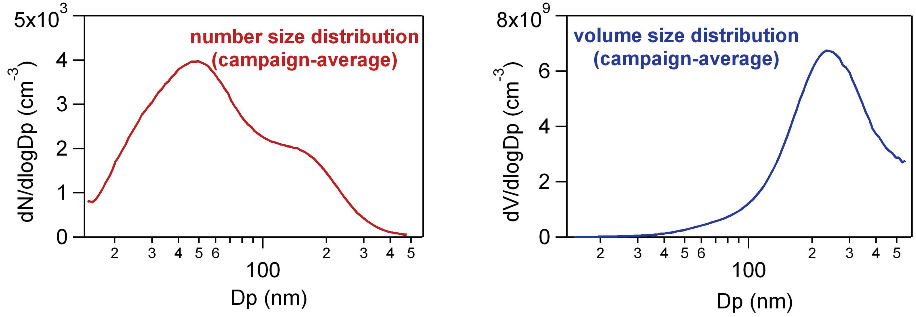

Fig. 4. Campaign-average number (left) and volume (right) size distributions for FAME-09. The particle size distributions were more variable and the particles were smaller on average during FAME-09 than during FAME-08.

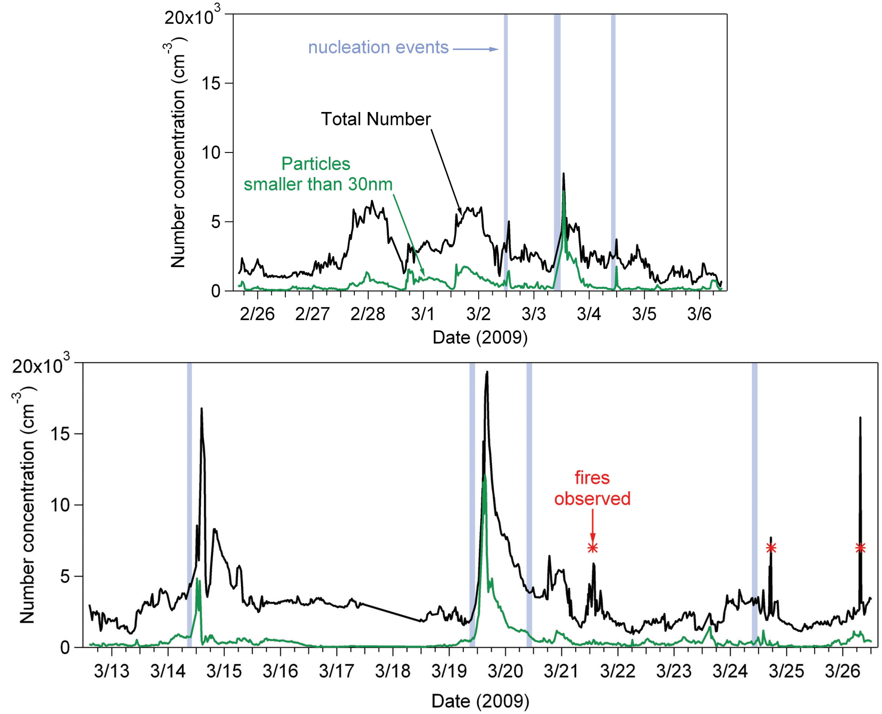

Fig. 5. Time series of total particle number (15 nm $< D_p <$ 500 nm) and particles smaller than 30 nm (15 nm $< D_p <$ 30 nm) measured by the SMPS. Nucleation events (light blue bands) were identified based on the increase in the total concentration of air ions (2 nm $< D_p <$ 10 nm). The time delay between these nucleation events and the increase in small-particle concentration from the SMPS is caused by the growth of the particles to the SMPS size range. On 24 March, the nucleated particles did not grow to the SMPS size range. Fires observed from the field site (red stars) are characterized by increases in larger particles. SMPS data was not available 6–12 March.

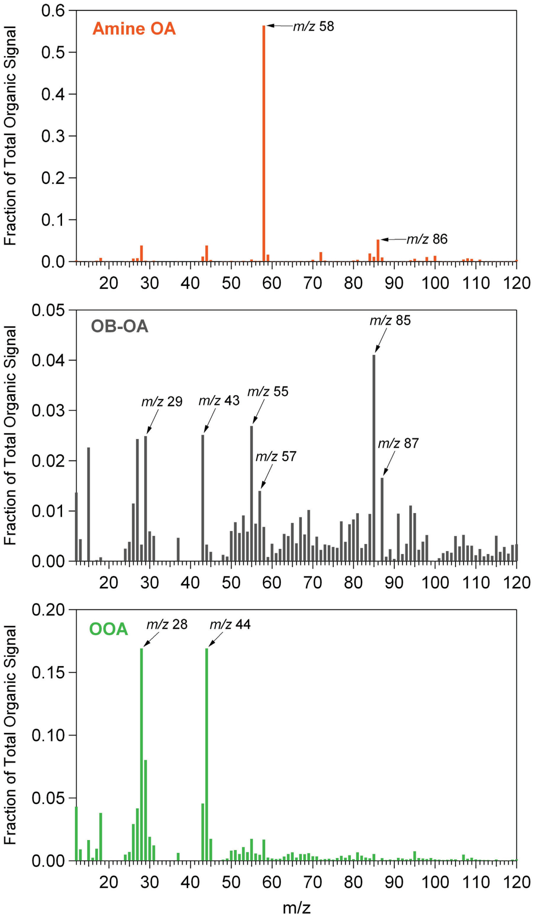

Fig. 6. Mass spectra of OA components from the 3-factor PMF solution.

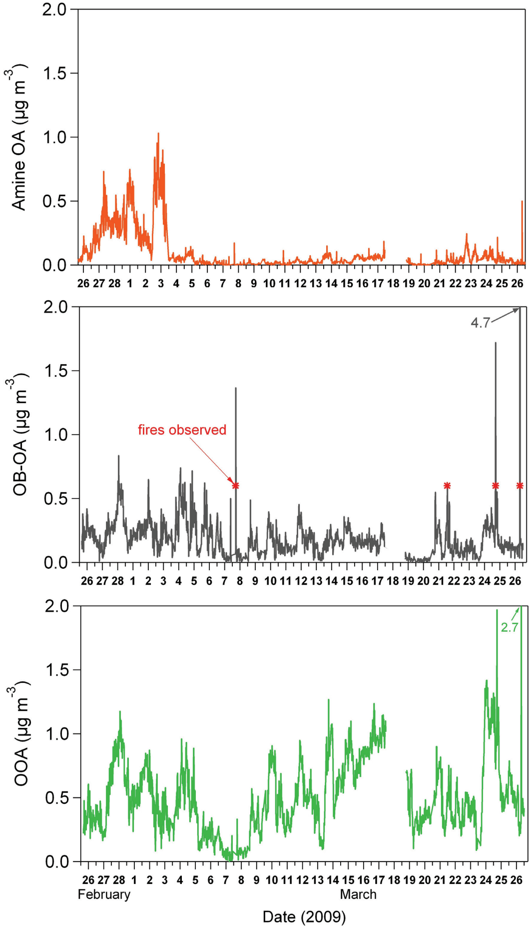

Fig. 7. Time series of OA components from the 3-factor PMF solution.

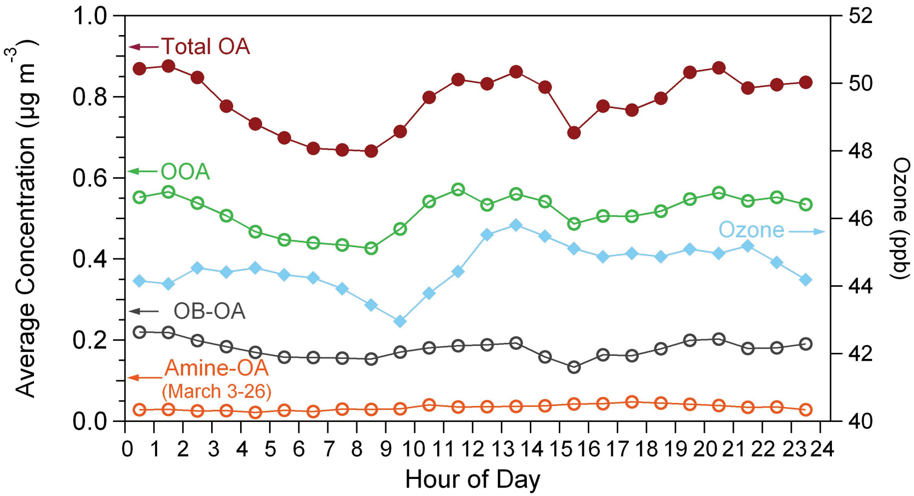

Fig. 8. Diurnal cycles of Total OA and OA component concentrations (left vertical axis) and of the ozone concentrations (right vertical axis). Ozone and OOA follow similar diurnal cycles.

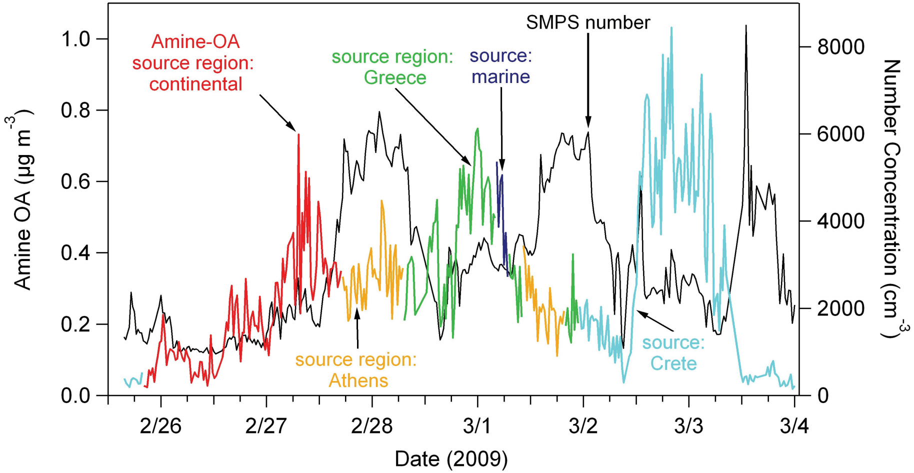

Fig. 9. Zoom of Amine-OA time series (left vertical axis) colored by the source region categorized as explained in the text. SMPS number concentrations (right vertical axis) do not correlate with Amine-OA concentrations.

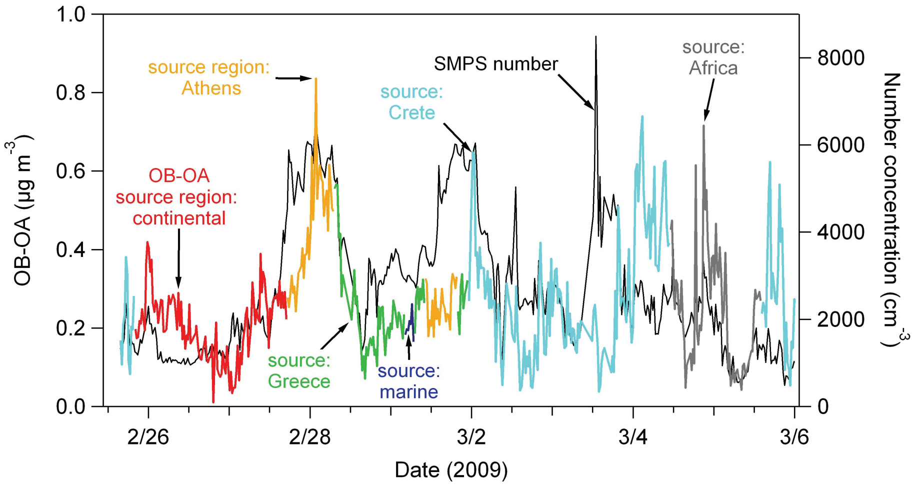

Fig. 10. Zoom of OB-OA time series (left vertical axis) colored by the source region categorized as explained in the text. SMPS number concentrations (right vertical axis) do not correlate with OB-OA concentrations.

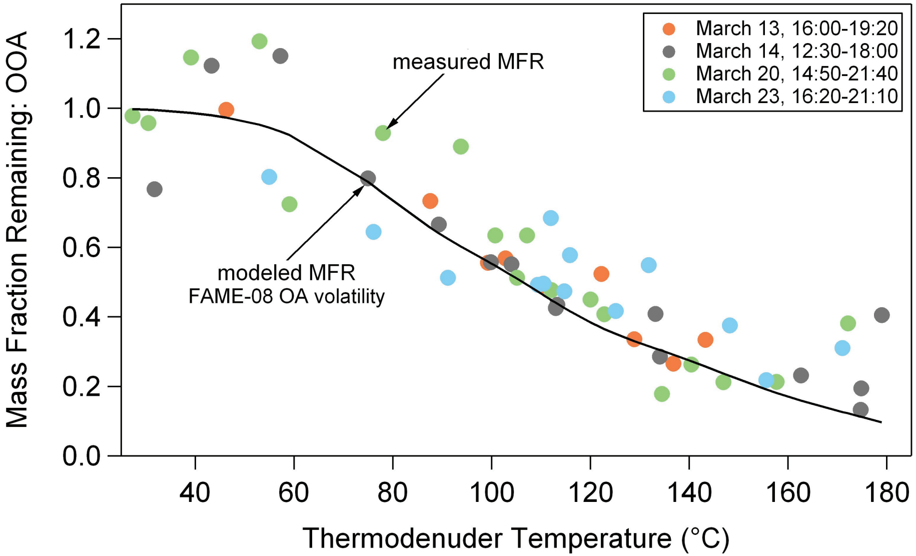

Fig. 11. Measured (circles) and modeled (line) OOA mass fraction remaining as a function of thermodenuder temperature. The modeled MFR is obtained using the FAME-08 OA volatility and the aerosol evaporation model. The volatility of the OOA measured during FAME-09 is the same as the volatility of the OA measured during FAME-08.

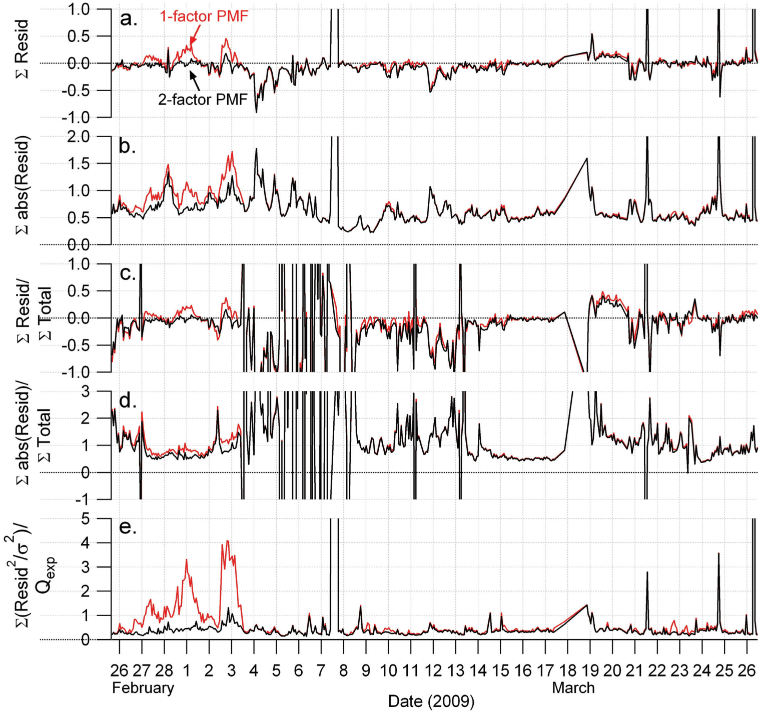

Fig. A1. Model residuals, $\mathbf{E} = \mathbf{X} - \mathbf{GF}$, for the 1-factor (red lines) and the 2-factor (black lines) PMF solutions as a function of time (summed over all *m/z*'s) calculated in five different ways: **(a)** sum of residuals **(b)** sum of the absolute value of residuals, **(c)** sum of residuals relative to total organics, **(d)** sum of absolute value of residuals relative to total organics, and **(e)** sum of squared, uncertainty-weighted ("scaled") residuals, $Q(t) = E(t)/S(t)$, relative to expected values, $Q_{\mathrm{exp}}(t)$. Plots obtained with the PMF evaluation tool, PET, by Ulbrich et al. (2009). The structure in the residuals is decreased significantly in the $p = 2$ solution compared to the $p = 1$ solution, especially during the first week of the campaign. Low OA concentrations result in high values for (**c** and **d**) during 4–9 March.

Title Page
Abstract Introduction
Conclusions References
Tables Figures
◀I ▶I
◀ ▶
Back Close
Full Screen / Esc
Printer-friendly Version
Interactive Discussion

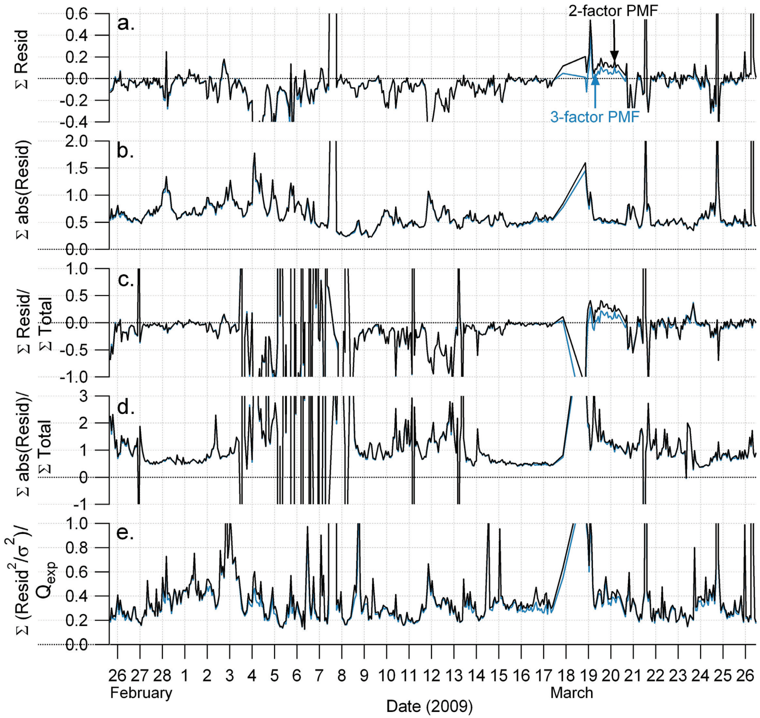

Fig. A2. Model residuals, $\mathbf{E} = \mathbf{X} - \mathbf{GF}$, for the 2-factor (black lines) and the 3-factor (blue lines) PMF solutions as a function of time (summed over all *m/z*'s) calculated in five different ways: **(a)** sum of residuals **(b)** sum of the absolute value of residuals, **(c)** sum of residuals relative to total organics, **(d)** sum of absolute value of residuals relative to total organics, and **(e)** sum of squared, uncertainty-weighted ("scaled") residuals, $Q(t) = E(t)/S(t)$, relative to expected values, $Q_{\mathrm{exp}}(t)$. Plots obtained with the PMF evaluation tool, PET, by Ulbrich et al. (2009). The structure in the residuals is decreased somewhat in the $p = 3$ solution compared to the $p = 2$ solution, especially during the period of 19–21 March. Low OA concentrations result in high values for (**c** and **d**) during 4–9 March.